Journal of Catalysis 280 (2011) 17–27

Contents lists available at ScienceDirect

Journal of Catalysis

journal homepage: www.elsevier.com/locate/jcat

Conversion of furfural and 2-methylpentanal on Pd/SiO_2 and $Pd–Cu/SiO_2$ catalysts

Surapas Sitthisa, Trung Pham, Teerawit Prasomsri, Tawan Sooknoi, Richard G. Mallinson, Daniel E. Resasco *

School of Chemical, Biological, and Materials Engineering, Center for Biomass Refining, University of Oklahoma, Norman, OK 73019, United States

ARTICLE INFO

Article history:
Received 15 October 2010
Revised 28 December 2010
Accepted 14 February 2011
Available online 16 April 2011

Keywords:
Pd catalyst
Bimetallic PdCu catalyst
Hydrogenation
Decarbonylation
Furfural
2-Methylpentanal

ABSTRACT

The conversion of furfural (FAL) and 2-methylpentanal (MPAL) under hydrogen has been studied over silica-supported monometallic Pd and bimetallic Pd–Cu catalysts. At low space times, the conversion of MPAL yields primarily pentane (decarbonylation), but at higher space times, di-methylpentyl ether (etherification) becomes the main product. Upon addition of Cu, both the overall activity and the decarbonylation selectivity decrease while the selectivity to hydrogenation and etherification increases. In contrast to MPAL, the conversion of FAL shows no etherification products at any space time in the temperature range 210–250 °C but only produces furan via decarbonylation. It is proposed that the presence of the aromatic ring in the furfural molecule has a marked effect in inhibiting the formation of the alkoxide surface intermediate, which is required in the etherification reaction. Density Functional Theory (DFT) calculations of furfural and 2-methyl pentanal have been conducted to gain a better understanding of the differences in the molecule–surface interactions between the aldehydes and the Pd and Pd–Cu surfaces. The reaction mechanisms and the resulting selectivity towards the possible reaction paths (hydrogenation/etherification/decarbonylation) are discussed in terms of the relative stability of the η^2-(C,O) and acyl surface species occurring on the different metal surfaces.

Published by Elsevier Inc.

1. Introduction

Fast pyrolysis [1–6] is an economically and technologically attractive method for conversion of lignocellulosic biomass [7–11]. However, the bio-oil obtained from this process has a relatively low heating value and typically contains a complex mixture of acids, alcohols, aldehydes, esters, ketones, phenols, furans, other oxygenated aromatics, alkenes, sugars as well as nitrogen compounds, and heavier oxygenates [12]. The characteristically high viscosity, corrosiveness, and low chemical/thermal instability limit the storability and processability of these oils [13]. Catalytic upgrading is required to stabilize bio-oils and make them fungible with conventional transportation fuels [14]. Among the large number of different oxygenates in bio-oils aldehydes are particularly undesirable as fuel components due to their high reactivity.

Hydrogenation of aldehydes to alcohols has been investigated over different metal catalysts [15–23]. Group Ib metals such as Cu can readily catalyze hydrogenation of furfural to furfuryl alcohol, with low yields of 2-methyl furan, the product of decarbonylation, only seen at high temperatures and with high metal loadings [24,25]. Alternatively, Group VIII metals such as Pd exhibit much higher activity for decarbonylation [26].

The main difference between Cu and Pd is that, upon aldehyde adsorption, the former only leads to formation of C-O-M (top, η^1-(O)) surface species, while the latter can stabilize both di-coordinated η^2-(C,O) and acyl η^1-(C) intermediates that lead to decarbonylation. In previous work [27] we showed that Pd not only catalyzes hydrogenation and decarbonylation of 2-methylpentanal, but also etherification. Interestingly, etherification was found to predominantly occur at high Pd loadings and after high temperature reduction treatments. It was also found that this is enhanced in the presence of the alcohol. Therefore, it was proposed that etherification requires a large ensemble of Pd atoms and the simultaneous formation of di-coordinated η^2-(C,O) and alkoxide intermediates (from adsorbed alcohol) [27]. Since decarbonylation may also require a large ensemble of atoms, one could speculate that it is possible to increase the etherification/decarbonylation ratio by alloying Pd with a metal, such as Cu, which is not active for decarbonylation, but can form alkoxide intermediates from alcohol.

In the present contribution, we have investigated the hydrogenation, decarbonylation, and etherification of aldehydes on Pd and Pd–Cu catalysts. To predict the aldehyde adsorbed species that can be formed on both Pd and Pd–Cu surfaces, DFT calculations were performed. In particular, we compare here the reactivity of two different aldehydes, furfural and 2-methyl-pentanal, which not only exhibit interesting differences in their chemical behavior, but represent aldehydes that are of importance in the upgrading of renewable fuels. Furfural is produced both during pyrolysis of cellulose and in the dehydration of sugars [28,29]. 2-Methyl-pentanal is formed upon aldol condensation and hydrogenation of propanal,

* Corresponding author.
E-mail address: resasco@ou.edu (D.E. Resasco).

0021-9517/$ - see front matter Published by Elsevier Inc.
doi:10.1016/j.jcat.2011.02.006

which also can be obtained from glycerol, a biodiesel by-product [30].

2. Experimental

2.1. Catalyst preparation

Pd/SiO_2 and $Pd–Cu/SiO_2$ catalysts with varying metal loadings were prepared by incipient wetness co-impregnation with aqueous solutions of the corresponding metal precursors ($Pd(NO_3)_2$ and $Cu(NO_3)_2{\cdot}H_2O$, Sigma Aldrich). Precipitated silica (HiSil 210, PPG Co.) having a BET surface area of 124 m^2/g was employed as support. A liquid/silica ratio of 1.26 ml/g was used to achieve incipient wetness for all samples. The Pd loadings were 5.0 and 0.5 wt% for the conversion of 2-methyl pentanal and furfural, respectively. After impregnation and drying in air at room temperature, the samples were further dried overnight at 110 °C and calcined under 100 ml/min flow of air at 400 °C for 4 h.

2.2. Catalyst characterization

2.2.1. Temperature programmed reduction

For each TPR measurement, 50 mg of catalyst was placed in a quartz tube, heated at 20 °C/min under 20 ml/min He flow up to 550 °C, and held at that temperature for 1 h. The sample was then cooled down to 0 °C and exposed to a stream of 5% H_2/Ar (Airgas Co.) at a flow rate of 20 ml/min while heating at 10 °C/min up to 600 °C. The amount of hydrogen uptake was monitored on-line by a TCD detector (SRI model 110) and recorded as a function of temperature.

2.2.2. Carbon monoxide chemisorption

The fraction of Pd exposed (CO/Pd) was estimated from dynamic CO chemisorption, measured in a pulse system equipped with Thermal Conductivity Detector (TCD). Before chemisorption, all catalysts were reduced in situ under pure H_2 flow by heating up to 200 °C with a heating rate of 10 °C/min, held for 1 h, purged with He for 30 min, and cooled to room temperature. Multiple pulses of 5% CO/He mixture were sent over the catalyst from a 100 μL sample loop until a constant CO peak area was observed. The exposed metal fraction (CO/Pd) was calculated from the moles of adsorbed CO per total moles of Pd impregnated onto the catalyst support.

2.2.3. DRIFTS of adsorbed CO

DRIFTS experiments were carried out in a Perkin Elmer Spectrum 100 FTIR spectrometer equipped with an MCT detector and a high temperature, low pressure chamber (HVC-DRP) fitted with KBr windows (Harrick Scientific Products, Inc.). In each measurement, 50 mg of catalyst was loaded to the DRIFTS chamber and reduced under 30 ml/min H_2 flow at a heating rate of 10 °C/min to 250 °C. Reduction was conducted for 1 h, then the sample was flushed with He for 30 min before cooling down to room temperature. A flow of 5% CO in He was passed through the chamber for 30 min at room temperature. Then, the chamber was flushed with He for 20 min before collecting and averaging 256 scans at 4 cm^{-1} resolution.

2.2.4. X-ray photoelectron spectroscopy (XPS)

XPS spectra were acquired on a Physical Electronics PHI 5800 ESCA system using an Al Kα X-ray anode at 35 W and 15 kV at a base pressure of about 1.0×10^{-8} Torr and using typical conditions for electron take-off angle (45°) with respect to the sample surface, spot size (400 μm), and pass energy (187.85 eV). The catalyst samples were pre-reduced ex situ under flow of H_2 (100 ml/min) at 400 °C for 1 h and then transferred into the XPS cell under He atmosphere to avoid exposure to air.

2.3. Catalytic activity measurements

The reactions of the two aldehydes (FAL and MPAL) were carried out in a tubular flow reactor. The pelletized and sieved catalyst (size 250–425 μm) was placed at the center of a quartz tube reactor, between two layers of glass bead and quartz wool, installed vertically inside an electric furnace. Prior to the reaction, the catalyst was pre-reduced under flow of H_2 (60 ml/min, Airgas 99.99%) for 1 h at 250 °C. After reduction, the catalyst was cooled down to the reaction temperature and the feed introduced continuously via a syringe pump (Cole Palmer). To keep all the compounds in the vapor phase all lines before and after the reactor were kept heated at 220 °C using heating tapes. The products were analyzed online on a gas chromatograph (Agilent model 6890) using HP-5 capillary column and FID detector. To vary the space time (W/F = catalyst mass/mass flow rate of reactant), the amount of catalyst was varied in the range 0.02–0.15 g, injecting liquid flows of 0.5 and 0.1 ml/hr for FAL and MPAL, respectively, into a hydrogen stream, and keeping the molar ratios H_2:FAL and H_2:MPAL at 25:1 and 12:1, respectively.

2.4. Computational method

Density functional theory (DFT) calculations were performed to investigate optimized structures and the adsorption energies (E_{ads}) of molecular adsorption of 2-methylpentanal (MPAL) and furfural (FAL) on Pd and Pd–Cu surfaces. Spin-polarized periodic DFT calculations were performed using the Vienna *ab initio* simulation package (VASP) [31–35], in which the Kohn–Sham equations are solved by self-consistent algorithms. The valence electrons were described by plane wave basis sets with a cutoff energy of 300 eV and the core electrons were replaced by the projector augmented wave (PAW) pseudo-potentials [36,37] to improve the computational efficiency. The Brillouin zone was sampled with a $3 \times 3 \times 1$ Monkhorst–Pack k-point mesh. The exchange–correlation functional was described within the generalized gradient approximation (GGA) proposed by Perdew, Burke and Ernzerhof (PBE) [38].

The Methfessel–Paxon method was employed to determine electron occupancies with a smearing width of 0.2 eV. Both Pd(1 1 1) and PdCu(1 1 1) slab models were constructed based on a 4×4 unit cell with lattice constants of 3.950 and 3.757 Å [39], respectively. The slab model consists of three metal layers with an ~18 Å vacuum gap in the direction perpendicular to the surface. Surface adsorption of molecules was modeled as taking place on the topmost layer of the slab. All of the atoms of the adsorbates were allowed to relax to their optimized positions, while those of the metal slab were kept frozen in the originally optimized position. The model was relaxed until the forces were convergent to 0.03 eV/Å.

The adsorption energy, E_{ads}, was calculated from the equation,

$$E_{ads} = E_{slab/ads} - E_{slab} - E_{gas}$$

in which $E_{slab/ads}$ is the total energy of the slab with adsorbates, E_{slab} is the energy of the slab, and E_{gas} is the energy of each adsorbate in the gas phase.

3. Results

3.1. Catalyst characterization

3.1.1. Temperature programmed reduction (TPR)

The TPR profiles of the monometallic Pd/SiO_2 and Cu/SiO_2 and the bimetallic $Pd–Cu/SiO_2$ catalysts are compared in Fig. 1. As

previously observed, supported Pd is much more easily reduced than Cu. In fact, while the reduction of Pd/SiO_2 is complete below 100 °C [40,41], Cu/SiO_2 shows two reduction peaks at 250 °C and 325 °C [42]. As proposed in many previous studies [43–46], the formation of an alloy in bimetallic Cu–Pd catalyst can be made evident by the appearance of an additional broad peak located between the reduction temperature of Pd and Cu It is also seen that the intensity of this peak increases with Cu content, while that in the position of unalloyed Pd diminishes. From the TPR results, it can be concluded that on the 0.5 Pd:0.5 Cu (% by weight) most of the Pd is forming an alloy with Cu, since the reduction peak corresponding to free-Pd has practically disappeared, in good agreement with previous TPR studies combined with X-ray absorption spectroscopy [43]. It is also worth noting that the presence of Pd increases the reducibility of Cu, leading to a shift toward lower temperatures.

3.1.2. DRIFTS of adsorbed CO

DRIFT spectra of adsorbed CO on the Pd monometallic and Pd–Cu bimetallic catalysts are shown in Fig. 2. On the pure Pd catalyst, the two characteristic bands at about 1967 and 2083 cm^{-1} are clearly seen, the former is typically associated to bridge and multiply bonded CO species, the latter to linearly adsorbed CO [47]. In line with previous reports [48–50] the bridge and multiply bonded CO species are greatly reduced, when even a small amount of the Group Ib metal is incorporated in the catalyst, typically explained in terms of the dilution of Pd ensembles [51,52]. In addition, as the Cu loading was increased, a new band was observed to grow at around 2118 cm^{-1}. This band has previously been assigned to CO weakly adsorbed on either Cu sites or bimetallic Pd–Cu sites [53]. The 35 cm^{-1} shift to higher wavenumbers relative to that of CO linearly adsorbed on pure Pd surfaces may be due to a perturbation of the electronic structure of Pd caused by the presence of Cu.

3.1.3. CO chemisorption

Table 1 summarizes the CO/Pd chemisorption data obtained on the Pd–Cu catalysts of varying Cu loading. The results show that the CO uptake is significantly reduced with the addition of Cu on Pd/SiO_2. It is clear that a significant fraction of the surface is covered by PdCu, which has a weaker interaction with CO compared to pure Pd, as discussed above. These CO chemisorption results are also consistent with TPD-HREEL studies by Jeroro et al. [54], which show that the addition of Cu to Pd(1 1 1) resulted in a slight decrease in the area of the CO desorption peak as well as a small shift in the desorption temperature from 470 K to 465 K.

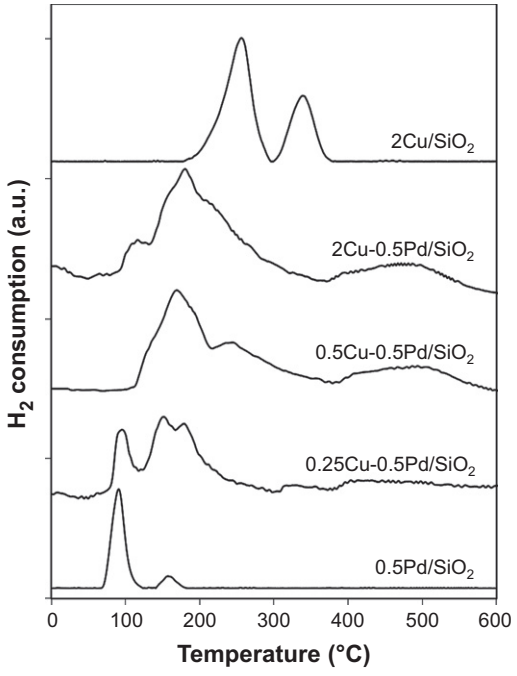

Fig. 1. Temperature programmed reduction profiles (TPR) of Pd and Pd–Cu catalysts.

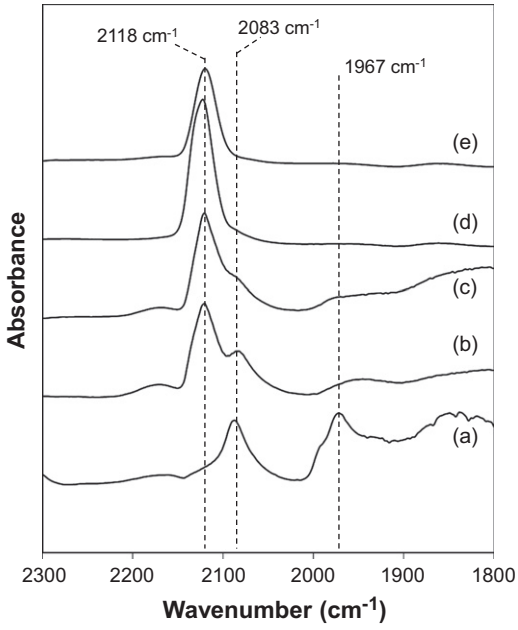

Fig. 2. Infrared spectra of CO adsorbed on (a) $0.5Pd/SiO_2$, (b) $0.25Cu–0.5Pd/SiO_2$, (c) $0.5Cu–0.5Pd/SiO_2$, (d) $2Cu–0.5Pd/SiO_2$ and (e) $0.5Cu/SiO_2$.

Table 1
Characteristics of the catalysts investigated.

Catalysts	Pd (wt%)	Cu (wt%)	CO/Pd ratio
5Pd	5	0	0.079
5Pd–0.25Cu	5	0.25	0.024
5Pd–2.5Cu	5	2.5	0.017

3.1.4. X-ray photoelectron spectroscopy (XPS)

The XPS spectra for the reduced Pd and Pd–Cu catalysts are shown in Fig. 3. While the catalysts were reduced ex situ and then transferred into the UHV chamber, it is clear that they remained reduced during the transfer since the observed binding energy for Pd $3d_{5/2}$ in the monometallic catalyst was 335.4 eV, in good agreement with those reported in the literature [55]. It is observed that the overall intensity of the Pd peaks decreased with the addition of Cu, indicating a lower degree of exposed Pd in the bimetallic catalyst. In addition, there is a broadening of the peaks, which indicate changes in binding energy of a fraction of the Pd. The XPS bands of PdCu catalysts were deconvoluted by imposing two restrictions to the fit, the Pd $3d_{5/2}$-to-$3d_{3/2}$ ratios were kept fixed at the value given by the relative multiplicity (2j + 1) and the energy separation between the two 3d peaks was kept the same for each Pd species proposed in the fit. Ruling out oxidation, this new peak may be attributed to electronic interactions between Pd and Cu, as discussed above. This result is consistent with XPS studies of bulk PdCu alloys obtained from Martensson et al. [56] which also show an increase (<1 eV) in binding energy for Pd $3d_{5/2}$ upon the addition of Cu compared to pure Pd.

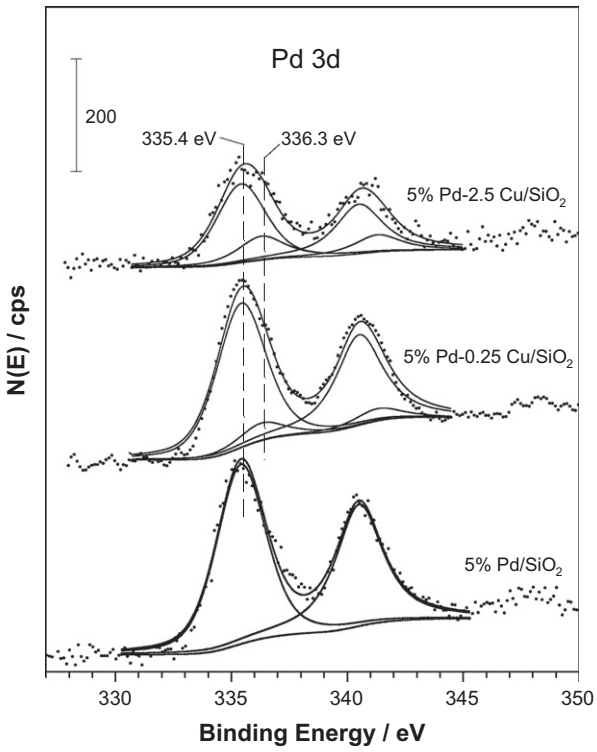

Fig. 3. X-ray photoelectron spectroscopy (XPS) of Pd_{3d} for different loadings of Cu in Pd/SiO_2 catalysts.

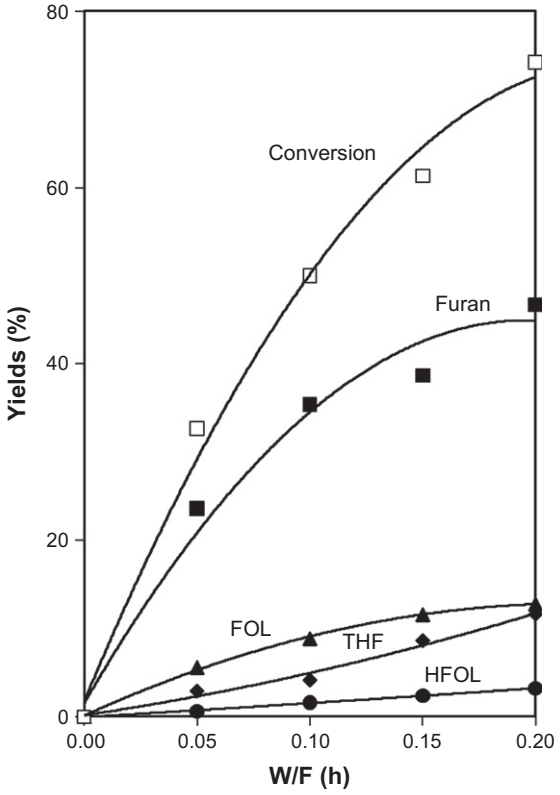

Fig. 4. Conversion and product distribution from furfural over 0.5%Pd/SiO_2 as a function of *W*/*F*. Temp = 230 °C, H_2/Feed ratio = 25, H_2 pressure = 1 atm, TOS = 15 min.

3.2. Reaction of aldehydes on Pd/SiO_2

The total conversion of furfural together with its product distribution is shown in Fig. 4 as a function of *W*/*F*. It is clear that the main reaction product at every *W*/*F* is furan, while furfuryl alcohol is observed from the lowest *W*/*F* as a minor product. In contrast, terahydrofuran (THF) and tetrahydro furfuryl alcohol (HFOL), formed as secondary products, are observed mostly at high *W*/*F*. In summary, furfural conversion on Pd can be described as two parallel routes: (i) decarbonylation to furan that subsequently hydrogenates to THF, and (ii) hydrogenation to furfuryl alcohol that subsequently hydrogenates to HFOL (Scheme 1).

As shown in Fig. 5, decarbonylation has a rather high activation energy and the yield of furan significantly increases at higher temperatures, while furfuryl alcohol is seen to increase with temperature and then to decrease, since as previously shown [57], the equilibrium conversion to furfuryl alcohol quickly decreases with temperature.

When the same 0.5%Pd/SiO_2 catalyst used for the reaction of furfural was tested for the reaction of methyl-pentanal almost no conversion was observed even at very high *W*/*F*, indicating a much lower reactivity of 2-methyl-pentanal on Pd compared to furfural. Therefore, to study the 2-methyl-pentanal conversion a higher-loading (5%Pd) catalyst was employed and the reaction was conducted at higher *W*/*F*. The total conversion of 2-methyl-pentanal and the corresponding product distribution are shown in Fig. 6 as a function of *W*/*F*. Upon increasing *W*/*F* from 1 to 5 h, the 2-methyl-pentanal conversion increases from 15% to 60%. While the activity level was much lower than that of furfural, the evolution of primary products was somewhat similar. That is, the main primary products were *n*-pentane (C5) and 2-methyl-pentanol (MPOL) that derive from direct decarbonylation and hydrogenation, respectively. An important difference with respect to furfural became apparent at higher *W*/*F*. It was observed that, as the conversion increased, an etherification product di-(methylpentyl) ether (DMPE) became dominant while the yields of C5 and 2-methyl-pentanol reached plateau. This behavior is clearly different from that observed with furfural, but has been observed before. In fact, in a previous study with 2-methyl-pentanal [27], we showed that using a high-metal-loading Pd catalyst (16% Pd/SiO_2) and low reaction temperatures (125 °C), formation of ethers is remarkably high.

Since in the present study we have used higher reaction temperature (210–250 °C) and lower Pd loading (0.5% Pd/SiO_2) with furfural compared to those with 2-methyl-pentanal, we conducted additional experiments to make the comparison more analogous. Furfural has a rather high boiling point (161.5 °C), therefore, to conduct the reaction low reaction temperatures (100 °C) a liquid-phase reactor was used. Also, to make a closer comparison to our previous study, a high-Pd-loading (5 wt%) catalyst was used. However, even under these conditions, no ether formation was detected. We conclude that the nature of the furfural molecule inhibits the etherification reaction.

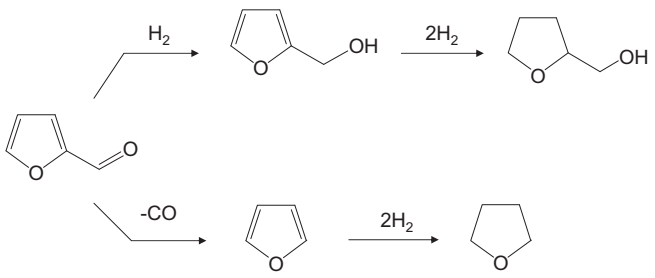

Scheme 1.

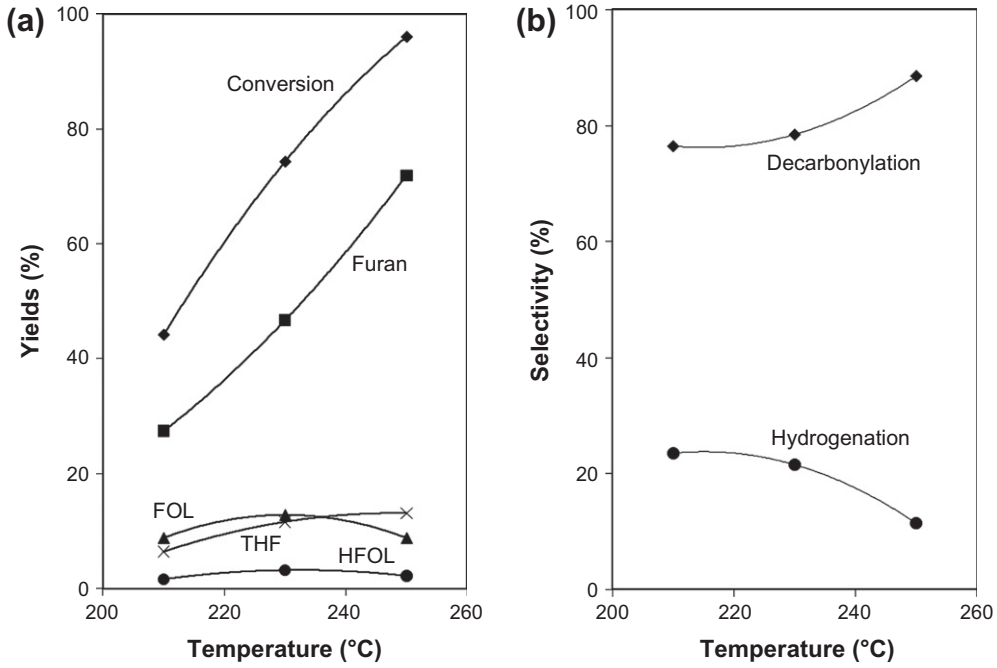

Fig. 5. (a) Yield and (b) selectivity of products from furfural conversion over 0.5%Pd/SiO_2 catalyst as a function of reaction temperature. W/F = 0.2 h, H_2/Feed ratio = 25, H_2 pressure = 1 atm, TOS = 15 min.

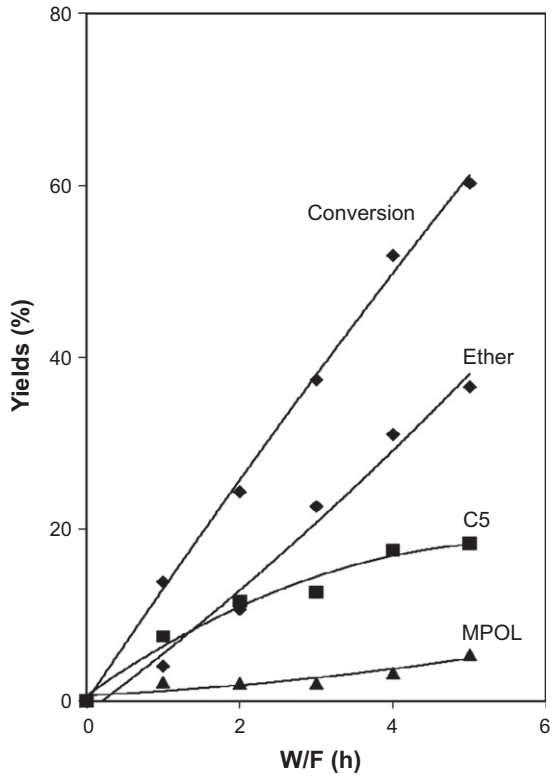

Fig. 6. Conversion and product distribution from 2-methyl-pentanal over 5%Pd/SiO_2 catalyst. Temp = 125 °C, H_2/Feed ratio = 12, H_2 pressure = 1 atm, TOS = 15 min.

In fact, in the case of the methyl-pentanal (MPAL) reaction, we have previously shown that MPAL reacts with MPOL forming a hemiacetal intermediate on the surface that readily converts to DMPE [27]. That is, the overall reaction pathways for 2-methyl-pentanal on Pd catalyst can be summarized as shown in Scheme 2.

We discuss below why we believe that an analogous reaction path for etherification is not favorable for furfural.

3.3. Reactions of aldehydes on bimetallic Pd–Cu/SiO_2

The effect of incorporating Cu to the catalysts has been studied for the same two reactions, furfural and 2-methyl-pentanal, described above. The results show that the total activity for FAL is decreased when the Cu metal was incorporated (Fig. 7a). This effect was also found when using 2-methyl-pentanal as a feed (Fig. 8a). Based on the TPR analysis, one can conclude that the addition of Cu leads to the formation of bimetallic Pd–Cu alloys. Similarly, the frequency shifts in DRIFT of adsorbed CO indicate that the addition of Cu results in a weaker binding of CO to the surface than on pure Pd. This weakening can be ascribed to a lower extent of electron back-donation from the metal to the π^* orbital of the CO molecule. While CO interacts with the surface through its C end and the aldehyde involves both C and O, it is reasonable to speculate that the electron back-donation from the metal to the carbonyl π^* orbital should be weaker on the Pd–Cu alloy than on pure Pd. A lower heat of adsorption of the aldehyde on the bimetallic catalyst, not only would cause a lower conversion, but as discussed below, a change in product distribution.

In fact, in both cases, with FAL and MPAL feeds, the yield of the decarbonylation products, furan and pentane, respectively, was greatly reduced, while the yield of hydrogenated products (FOL and MPOL) significantly increased as a function of Cu loading (Figs. 7a and 8a). As shown in Fig. 9, no significant hydrogenation activity was observed for Cu alone under these conditions.

3.4. DFT calculations of 2-methylpentanal (MPAL) and furfural (FAL) adsorption on Pd(1 1 1) and PdCu(1 1 1) slabs

DFT calculations were performed to compare the adsorption energetic for MPAL and FAL on both Pd(1 1 1) and PdCu(1 1 1) slabs. Calculating the adsorption of such large molecules is complicated because the system exhibits numerous possible configurations.

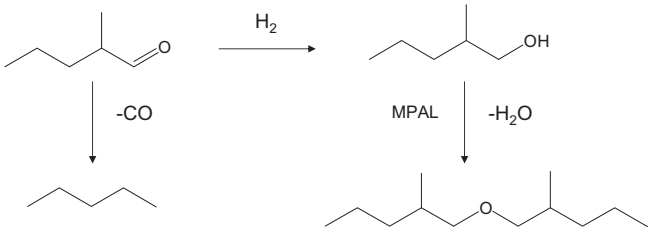

Scheme 2.

We have selected the ones that we believe are most relevant for catalysis. To minimize the effect of adsorbate–adsorbate intermolecular interactions, we have chosen a low-coverage surface (1/16 ML) by using a relatively large unit cell (4×4).

The optimized structures of MPAL in the gas phase and on the various surfaces are illustrated in Fig. 10. The corresponding adsorption energies (E_{ads}) and bond lengths are summarized in Table 2. The calculations show that on Pd(1 1 1), the adsorption of the MPAL molecule occurs via the carbonyl group, interacting with the surface in a η^2-(C,O) configuration, in which both C and O atoms of the carbonyl group are linked to the metal surface, while the aliphatic hydrocarbon part remains away from the surface. This theoretical result is consistent with the HEELS results obtained from Shekhar et al. [58], which have shown that the η^2-(C,O) aldehyde is the dominant species observed on clean Pd surfaces, with some η^1 species appearing only at low temperatures. As summarized in Table 2, the adsorption energy for MPAL on Pd(1 1 1) is 27.0 kJ/mol. Also, it is worth noting that the length of the C–O bond, d_1, in the adsorbed state is 0.06 Å longer than that in the gas phase, which may be ascribed to the interaction of the carbonyl π bond with the Pd(1 1 1) surface (i.e. electron back-donation). In contrast, the lengths for the other bonds d_2, d_3, d_4, d_5, and d_6 remain unchanged, indicating a low extent of interaction. A similar calculation was conducted for furfural (FAL). The optimized structures of FAL in the gas phase and adsorbed on the different surfaces are illustrated in Fig. 11. The corresponding adsorption energies (E_{ads}) and bond lengths are summarized in Table 3.

On Pd(1 1 1), the presence of the aromatic ring in FAL plays a crucial role in promoting a flat adsorption on the surface. This results in a twofold increase in heat of adsorption of FAL (55.4 kJ/mol, Fig. 11b) compared to MPAL (27.0 kJ/mol, Fig. 10b). This result is consistent with DFT calculations of furan adsorption on Pd(1 1 1) made by Bradley et al. [59], who showed that preferred adsorption is with the ring essentially parallel to the surface. As opposed to the results for Pd, our recent DFT calculations of FAL on a Cu(1 1 1) surface [57] have shown a strong repulsion between the furan ring and the Cu(1 1 1) surface, due to the overlap of the 3d band of the surface Cu atoms and the aromatic furan ring. As a result, the adsorption of FAL on Cu(1 1 1) is weak and can only occur in the η^1(O)-aldehyde configuration, via the carbonyl O atom.

A similar comparison of the DFT results can be made for MPAL and FAL over the PdCu(1 1 1) surface. It is clearly seen that the presence of Cu significantly reduces the interaction of both aldehydes with the metal surface. Relative to those on the pure Pd, the heats of adsorption on the bimetallic surface are significantly reduced. That is, the adsorption strength of MPAL drops from 27.0 kJ/mol on Pd(1 1 1) to 12.4 kJ/mol on PdCu(1 1 1). Moreover, the heat of adsorption of FAL changes from 55.4 kJ/mol on Pd(1 1 1) to 9.6 kJ/mol on PdCu(1 1 1). This dramatic reduction in the strength of interaction can be ascribed to the effect of the aromatic ring, which has a strong affinity for Pd, but not for Cu.

Another aspect important to discuss is the significant changes in strength of interaction observed with respect to the place in which the molecule is adsorbed on PdCu(1 1 1). For instance, in the case of MPAL, the η^2-(C–O) aldehyde adsorption with the C atom on top of Pd and the O atom on Cu (see Fig. 10c) results in a higher adsorption energy (12.4 kJ/mol) than the other configurations (i.e. C/Cu–O/Pd or C/Pd–O/Pd). The preferential adsorption mode results in greater elongation of the carbonyl bond, d_1. Again, as in the case of pure Pd, the lengths of the other bonds (d_3, d_4, d_5, and d_6) remain unmodified upon adsorption. In addition, the dis-

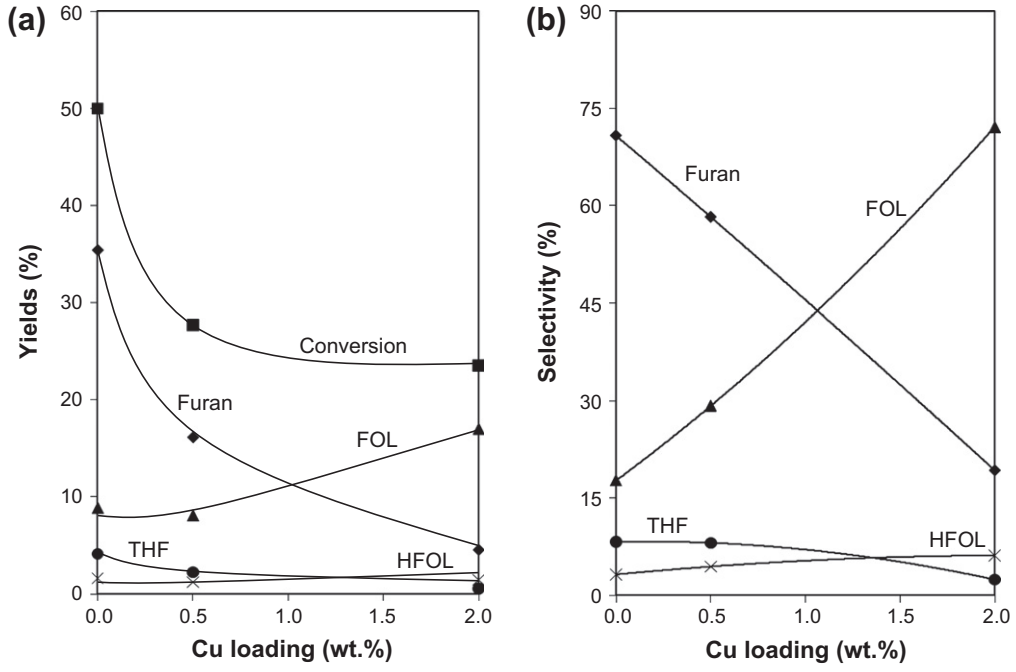

Fig. 7. (a) Yield and (b) selectivity of products from the reaction of furfural on Pd/SiO_2 as a function of Cu loading. W/F = 0.1 h, Temp = 230 °C, H_2/Feed ratio = 25, H_2 pressure = 1 atm, TOS = 15 min.

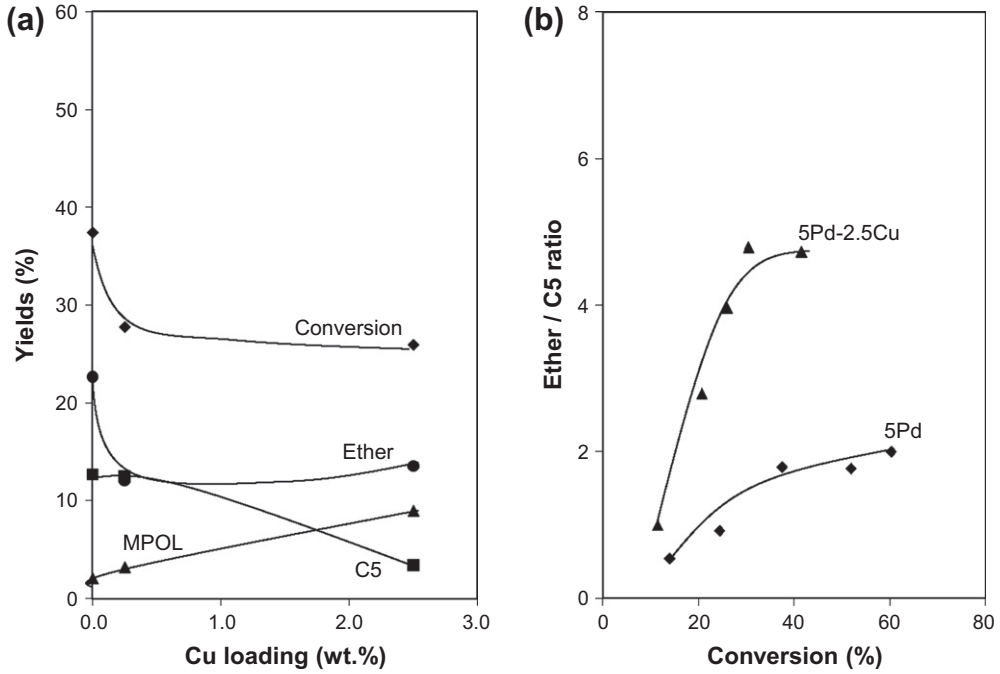

Fig. 8. (a) Yield of products from the reaction of 2-methyl-pentanal on Pd/SiO_2 as a function of Cu loading. W/F = 3 h, Temp = 125 °C, H_2/Feed ratio = 12, H_2 pressure = 1 atm, TOS = 15 min. (b) Ether/C_5 ratio as a function of conversion for Pd/SiO_2 and $Pd–Cu/SiO_2$ catalysts.

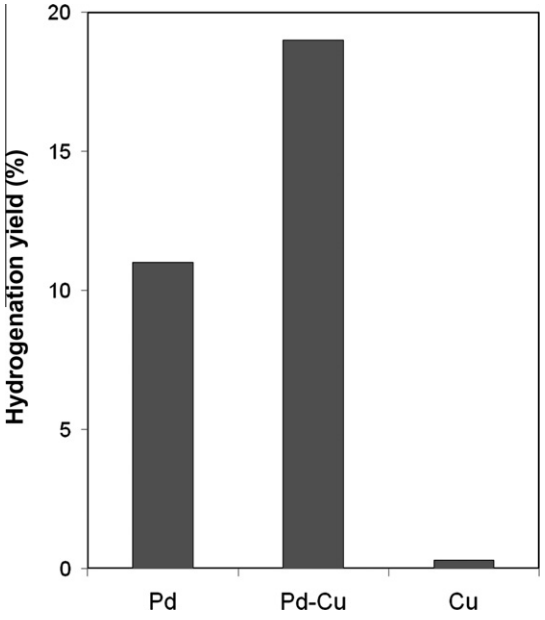

Fig. 9. Yield of hydrogenation products on $0.5Pd/SiO_2$, $0.5Pd–0.5Cu/SiO_2$ and $0.5Cu/SiO_2$ catalysts. W/F = 0.2 h, Temp = 250 °C, H_2/Feed ratio = 25, H_2 pressure = 1 atm, TOS = 15 min.

tances between C or O and the surface are significantly longer ~0.4–0.7 Å than those on Pd(1 1 1). This difference is in agreement with the trends in adsorption energy and the length of the C–O bond. A weaker interaction results in longer adsorbate–surface distances and shorter/stronger carbonyl bonds.

The case of FAL is somewhat different due to the important role played by the furanyl ring in the interaction with the surface. As mentioned above, on pure Pd the presence of the ring greatly enhances the interaction. However, when Cu atoms are added, the stability of the adsorbed FAL is dramatically decreased. In the case of FAL adsorbed on Pd(1 1 1), all bonds are elongated, particularly the C=O and C=C bonds. To investigate this interaction, various FAL/PdCu(1 1 1) configurations were simulated.

It is interesting to see the differences in the calculated energies and bond lengths as the molecule is placed on different places on the alloy surface. That is, while the heat of adsorption is much lower than on pure Pd, it is not as low when the O atoms in FAL are placed over a Cu atom and the furanyl ring over Pd atoms. By contrast, the adsorption energy is even lower when the ring is placed over Cu atoms. As shown on the side view of Fig. 11d, the molecule even bends away from the Cu atom due to the apparent repulsion.

4. Discussion

4.1. Reaction of aldehydes on Pd/SiO_2

The reaction pathways for furfuraldehyde and 2-methyl-pentanal conversion on Pd and PdCu surfaces have been investigated on silica-supported catalysts. To discuss the observed product distributions and their strong dependence on the catalyst formulation and type of aldehyde used as a feed, we should consider the following possible reaction paths (Scheme 3).

The starting interaction of the carbonyl compounds (**1**) with the Pd surface appears to involve a side-on complex ($\pi_{C=O}$) [60]. In the case of Pd, as discussed above, a rather extensive electron backdonation into the carbonyl group can occur. This interaction readily weakens the C–O bond, helping stabilizing a di-sigma complex (di-σ_{C-O}) (**2**), also known as η^2-(C–O) aldehyde. The formation of this species upon adsorption of saturated aldehydes (i.e. formaldehyde, acetaldehyde, and propionaldehyde) on Pd, Pt, Rh and Ru metal surfaces has been confirmed using high resolution electron energy loss spectroscopy (HREELS) [60–64]. Moreover, the η^2-(C–O) aldehyde (**2**) has been found to be a precursor for aldehyde hydrogenation over a Pd catalyst [58]. In contrast, on Cu catalysts the η^1-(O) aldehyde is known to be the main precursor for aldehyde hydrogenation [57,65]. In our present study, formation of

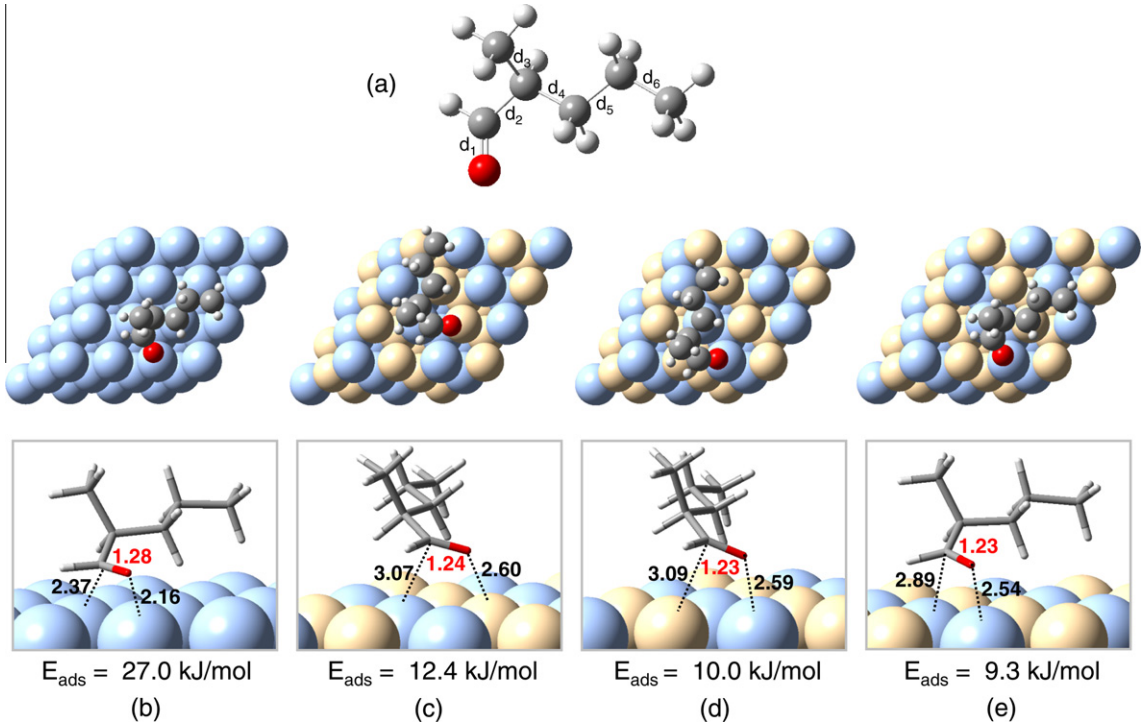

Fig. 10. DFT optimized structures of 2-methylpentanal (MPAL) in gas phase (a), and its adsorption on Pd(1 1 1) (b) and PdCu(1 1 1) (c–e) slabs. Red, gray, white, blue, and yellow spheres represent O, C, H, Pd and Cu atoms, respectively. The corresponding bond lengths are given in Table 2. (For interpretation of the references to colour in this figure legend, the reader is referred to the web version of this article.)

Table 2
Adsorption energies (kJ/mol) and optimized bond lengths (Å) of 2-methylpentanal on Pd(1 1 1) and PdCu(1 1 1) slabs (see Fig. 10).

Model	MPAL	MPAL/Pd(1 1 1)	MPAL/PdCu(1 1 1)		
	(a)	(b)	(c)	(d)	(e)
E_{ads}	–	27.0	12.4	10.0	9.3
d_1	1.22	1.28	1.24	1.23	1.23
d_2	1.52	1.52	1.51	1.51	1.51
d_3	1.54	1.54	1.54	1.54	1.54
d_4	1.53	1.53	1.53	1.53	1.53
d_5	1.53	1.53	1.53	1.53	1.53
d_6	1.53	1.53	1.53	1.53	1.53

alcohols via hydrogenation of either furfural or 2-methyl-pentanal was also observed as a minor reaction path. On the other hand, decarbonylation products (furan and pentane from FAL and MPAL, respectively) were dominant over Pd/SiO_2 even at the lowest W/F values.

The HREELS experiments of acetaldehyde adsorbed on clean Pt(1 1 1) [63] show that, at low temperatures, an η^2-(C–O) surface species was formed, but it was readily decomposed above 330 K, producing an acetyl intermediate (η^1(C)-acyl, (**3**)) that was stable up to 440 K. Consequently, it is conceivable that a similar acyl intermediate may be readily formed on Pd under our reaction conditions. In fact, as shown in Fig. 5, the decarbonylation product, furan, increases as a function of temperature.

In the presence of hydrogen, together with formation of the acyl intermediate that leads to decarbonylation, the η^2-(C–O) aldehyde (**2**) can be hydrogenated to the alkoxide complex (**4**) [66–70], which is the intermediate for the hydrogenated products (alcohol), i.e., MPOL produced from MPAL.

Formation of alkoxide intermediates from saturated aldehydes has been typically thought to occur via H attack to the carbonyl C of the η^2-(C–O) aldehyde [71]. In contrast, in the case of furfural, our recent mechanistic studies on Cu catalysts have shown that the first H attack may take place at the carbonyl O [57], which results in the formation of a hydroxyalkyl surface species. Our DFT calculations showed that this intermediate results in a somewhat lower energy barrier than the one involving the formation of the alkoxide intermediate. We have ascribed the higher stability of the hydroxyalkyl species to the stabilization role played by the conjugation with the aromatic furan ring [57]. Thus, in this case, it is more likely that the hydroxyalkyl species is the dominant intermediate in furfural hydrogenation. Therefore, a mechanism for furfural conversion over Pd catalysts can be proposed, as shown in Scheme 4.

In contrast to furfural, methyl pentanal does not have a conjugated system and therefore formation of a hydroxyalkyl species would not be favorable. In this case, the reaction would probably occur via an alkoxide species (**4**), as shown in Scheme 3, which would favor formation of the ether, as observed experimentally (see Fig. 6), particularly at high space times (W/F). As previously proposed [27,72], the η^2-(C–O) intermediate is readily stabilized on Pd at low temperatures and reacts with the alkoxide to form the ether, a bimolecular reaction that is facilitated on large Pd ensembles, i.e., maximum ether yield is obtained at low reaction temperatures on high-loading, large-particle Pd catalysts. With furfural, even under these optimum etherification conditions, no ether was observed.

4.2. Effect of Cu loading on Pd/SiO_2

The three characterization techniques used in this study, TPR, XPS, and DRIFTS, provide evidence for the formation of a Pd–Cu bimetallic phase. As shown in a number of studies [43–46,50], the clear shift in reduction temperature observed by TPR (higher than pure Pd and lower than pure Cu) is indicative of a direct metal–metal interaction.

Table 3
Adsorption energies (kJ/mol) and optimized bond lengths (Å) of furfural on Pd(1 1 1) and PdCu(1 1 1) slabs (see Fig. 11).

Model	FAL	FAL/Pd(1 1 1)	FAL/PdCu(1 1 1)		
	(a)	(b)	(c)	(d)	(e)
E_{ads}	–	55.4	9.6	7.4	4.0
d_1	1.23	1.31	1.30	1.28	1.23
d_2	1.46	1.47	1.47	1.45	1.46
d_3	1.39	1.44	1.42	1.41	1.39
d_4	1.43	1.44	1.44	1.42	1.43
d_5	1.38	1.45	1.37	1.44	1.38
d_6	1.37	1.40	1.39	1.40	1.37
d_7	1.39	1.40	1.39	1.40	1.39

In addition, XPS shows both a decrease in the relative intensity of Pd and the appearance of a high-binding energy state. The changes in intensity and binding energy observed by XPS indicate an extensive degree of Pd–Cu interaction. However, the exact nature of the electronic modification is complex. While Pd–Cu catalysts have been extensively investigated, the extent and direction of electron transfer between the two elements are still a matter of discussion [73,74]. In a theoretical study of Pd–Cu clusters, Fernandez-Garcia et al. [75] concluded that the metal–metal interaction not only includes electron transfer, but also a significant rehybridization. That is, while the net charge of Pd in the alloy is negative as a result of an electron transfer from Cu, the electronic population of the Pd 4d orbitals is lower in the alloy than in the pure metal. They indicate that two important effects are in apparent contradiction with the direction of the net electron transfer. First, the binding energy of the core levels is higher in the alloy (as observed experimentally), and the potential for back-donation from the d orbitals to an adsorbate is lower for the alloy than for the pure Pd. Lopez and Norskov [76] have shown that alloying Cu to Pd causes a change in the position of the d-band center of Pd relative to the Fermi level. They have calculated that the Pd d-band center for $Cu_3Pd(1\,1\,1)$ is shifted about 0.43 eV away from the Fermi level compared to the position of that in Pd(1 1 1) (i.e. −2.23 vs. −1.80 eV). This shift causes a lower extent of π-back-donation from Pd to CO, resulting in a weakening of CO adsorption on PdCu alloy surfaces, as observed experimentally. Therefore, regardless of the exact nature of the Pd–Cu interaction, the net effect of Cu addition is a decreased extent of back-donation and a weaker adsorption strength.

Finally, the shift of the linear C–O stretching vibration band to higher wavenumbers observed by DRIFTS upon Cu incorporation in the bimetallic Pd–Cu catalyst indicates a lower extent of electron back-donation from the metal to π^* states of the CO molecule compared to the pure Pd [77].

An analogous effect can be thought to occur in the interaction with the aldehydes in the η^2-(C–O) configuration. In the case of pure Pd, an efficient donation of electrons into the antibonding states of the carbonyl in the aldehyde enhances the strength of interaction with the metal, while it weakens the C–O bond. By contrast, a lower potential for back-donation in the alloy should result in a lower stability of the di-sigma surface aldehyde species η^2-(C–O) and an enhancement in the C–O bond strength compared to that in the pure Pd. This trend would explain the observed decrease in the conversion of FAL and MPAL as a function of Cu loading as seen in Figs. 7a and 8a, respectively.

In agreement with this proposal, our DFT calculations show that the η^2-(C–O) aldehyde is much less stable on the surface of the bimetallic PdCu(1 1 1) than on the pure Pd(1 1 1). For example, as shown in Fig. 10 for the case of MPAL, the distances between both C and O atoms of η^2-(C–O) are significantly longer, indicating an overall weaker interaction with the surface. Even when both C and O are bonded to two Pd atoms, the distances are about 20% longer than on the pure Pd(1 1 1). However, the difference is even larger when dissimilar atoms are used in the surface bond. In that case, while the M–O bond is still about 20% longer than in the case of the monometallic surface, the C–M bond becomes 30% longer,

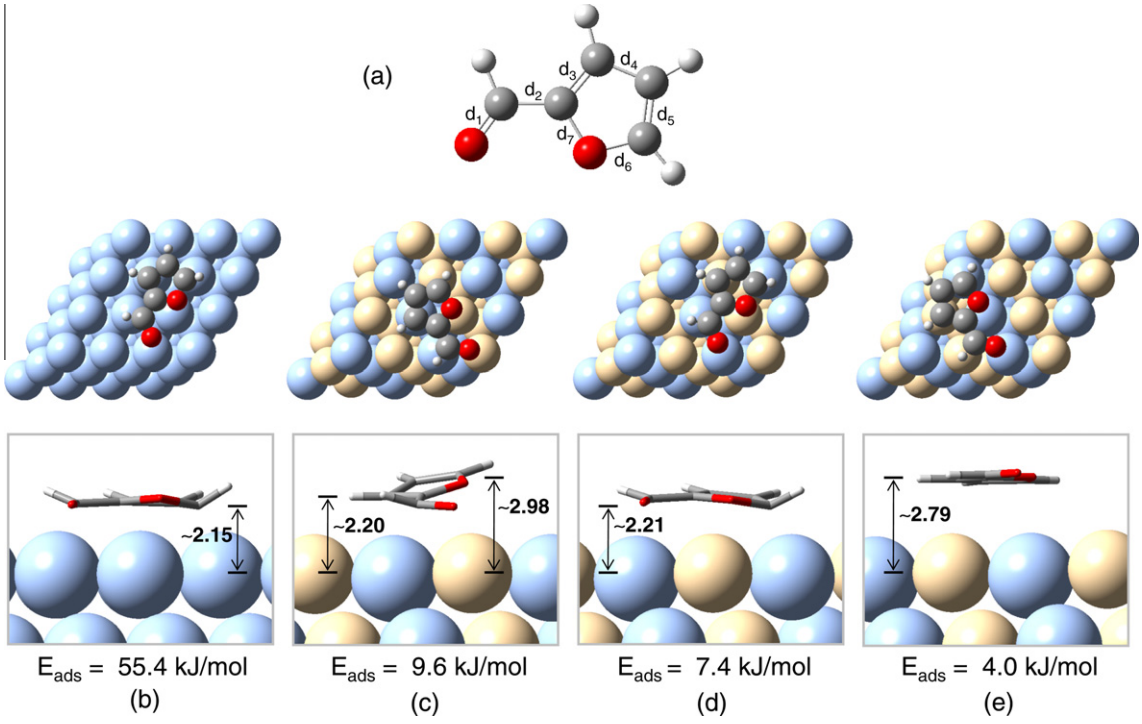

Fig. 11. DFT optimized structures of furfural (FAL) in gas phase (a), and its adsorption on Pd(1 1 1) (b) and PdCu(1 1 1) (c–e) slabs. Red, gray, white, blue, and yellow spheres represent O, C, H, Pd and Cu atoms, respectively. The corresponding bond lengths are given in Table 3. (For interpretation of the references to colour in this figure legend, the reader is referred to the web version of this article.)

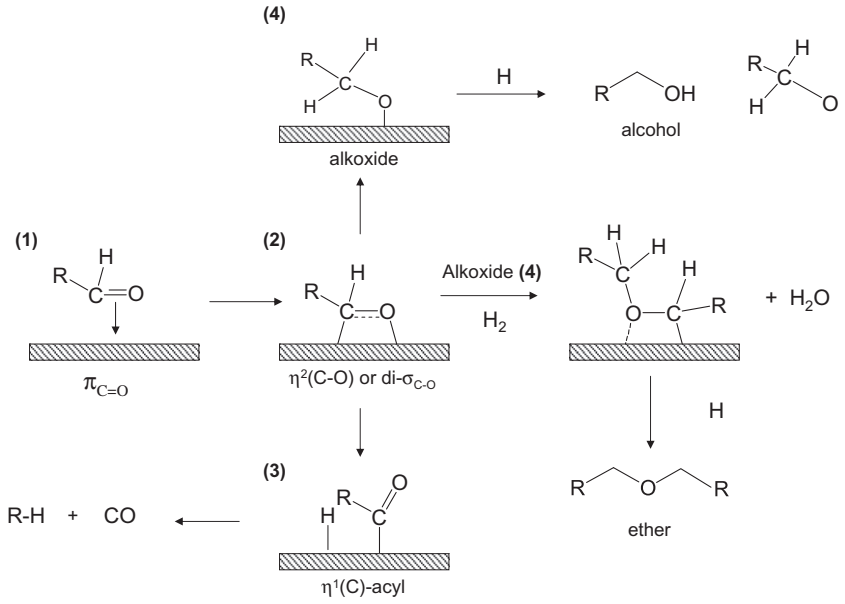

Scheme 3.

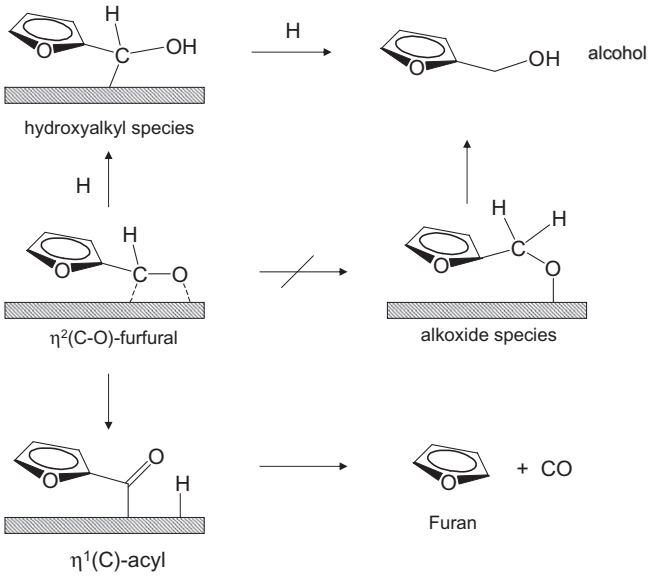

Scheme 4.

which makes the surface species resemble more an η^1-(O) than an η^2-(C–O). It is relevant to point out that on pure Cu surfaces, aldehydes adsorb exclusively in the η^1-(O) configuration [57], with the oxygen lone pair orbital acting as a Lewis base [60]. By contrast, on Group VIII metals both η^1 and η^2 have been observed at a ratio that depends on the type of metal [78]. For example, a higher η^2/η^1 ratio is observed on Ru compared to Pt. This difference has been ascribed to a higher extent of electron back-donation, resulting from the higher position of the Fermi level in Ru compared to Pt. Moreover, while η^2-(C–O) is dominant on clean Ru surfaces and even more so when electron-donating K is co-adsorbed, η^1-(O) is dominant on oxygen-covered Ru surfaces [79], which illustrates the importance of electronic effects in the nature of the adsorbed aldehyde species, as previously proposed by others [80,81].

In the case of the Pd–Cu alloys, as the stability of the di-sigma η^2-(C–O) species is decreased, we may expect that the interaction with the electronegative atom (i.e. the carbonyl O) will be favored, forming an intermediate similar to an η^1(O) aldehyde. Of great importance for explaining the observed selectivity is the realization that the long carbonyl C–metal distances predicted by DFT will greatly hinder the formation of the acyl intermediate, needed for decarbonylation. The drastic decrease in decarbonylation for both aldehydes (i.e. yields of furan and pentane) as a function of Cu loading (Fig. 7a and b) in the conversion of FAL and MPAL, respectively, is in perfect agreement with the proposed mechanism. In contrast to the decarbonylation route, hydrogenation may still occur if an η^1(O)-like intermediate is favored. In fact, it was observed that not only the selectivity but also the yield towards hydrogenated product (FOL and MPOL, respectively) was observed to increase at higher Cu contents. Finally, in the case of MPAL, as the formation of acyl species is suppressed, hydrogenation of the adsorbed aldehyde forming the alkoxide intermediate may lead to an increase in the ether selectivity, thus explaining the higher ether/C5 ratio observed for the Pd–Cu catalyst (Fig. 8b).

5. Conclusions

From the comparative study of the different reactions that furfural and methyl-pentanal undergo on Pd and Pd–Cu catalysts we draw the following conclusions:

(a) On pure Pd, decarbonylation is the dominant reaction for both types of aldehydes, even at low *W*/*F*. This behavior is due to the preferential formation of an acyl intermediate at higher temperatures, which can readily decompose into CO and hydrocarbons. This proposed trend explains the high decarbonylation/hydrogenation ratios obtained for both aldehydes on Pd.

(b) In the case of 2-methyl-pentanal, when large Pd ensembles are available, and the temperature is low enough, the reaction of the η^2-(C–O) aldehyde with an adjacent alkoxide becomes important to ether formation. This is not the case for furfural, for which hydrogenation may occur via a hydroxyalkyl intermediate, which is more stable than the alkoxide. As a result, there is no etherification with furfural.

(c) Incorporation of Cu onto Pd/SiO_2 catalyst results in the formation of Pd–Cu alloys, which may exhibit an electronic structure different from that of pure Pd. This electronic perturbation results in a lower extent of electron back-donation to the π^* system of the aldehydes. As a result, the formation of the side-on η^2-(C–O) aldehyde species is less stable on Pd–Cu than on pure Pd, which in turn makes the formation of the acyl intermediate less likely. Therefore, the decarbonylation rate is greatly reduced on PdCu catalysts, but the hydrogenation rate is increased.

Acknowledgments

This work was partially supported by the National Science Foundation EPSCOR (Grant 0814361), the Oklahoma Bioenergy Center, and the Department of Energy (Grant DE-FG36GO88064). Allocation of computing time provided by the OU Supercomputing Center for Education and Research (OSCER) at the University of Oklahoma is acknowledged. The XPS analysis was conducted by Dr. Min Shen and his support is gratefully acknowledged.

References

[1] A. Demirbas, Fuel Proc. Technol. 88 (2007) 591.
[2] V.R. Wiggers, A. Wisniewski Jr., L.A.S. Madureira, A.A. Chivanga Barros, H.F. Meier, Fuel Proc. Technol. 88 (2009) 2135.
[3] M.G. Perez, J. Shen, X.S. Wang, C.Z. Li, Fuel Proc. Technol. 91 (2010) 296.
[4] J. Lede, F. Broust, F.T. Ndiaye, M. Ferrer, Fuel 86 (2007) 1800.
[5] M. Asadullah, M.A. Rahman, M.M. Ali, M.S. Rahman, M.A. Motin, M.B. Sultan, M.R. Alam, Fuel 86 (2007) 2514.
[6] O. Onay, O.M. Kockar, Fuel 85 (2006) 1921.
[7] A. Zabaniotou, O. Ioannidou, V. Skoulou, Fuel 87 (2008) 1492.
[8] L.R. Lynd, J.H. Cushman, R.J. Nichols, C.E. Wyman, Science 251 (1991) 318.
[9] G.W. Huber, S. Iborra, A. Corma, Chem. Rev. 106 (2006) 4044.
[10] G.W. Huber, A. Corma, Angew. Chem. Int. Ed. 46 (2007) 7184.
[11] R.E.H. Sims, W. Mabee, J.N. Saddler, M. Taylor, Bioresour. Technol. 10 (2010) 1570.
[12] C. Amen-Chen, H. Pakdel, C. Roy, Biomass Bioenergy 79 (2001) 277.
[13] Y.H.E. Sheu, R.G. Anthony, E.J. Soltes, Fuel Process. Technol. 19 (1988) 31.
[14] A.V. Bridgwater, Appl. Catal. A: Gen. 16 (1994) 5.
[15] A. Ausavasukhi, T. Sooknoi, D.E. Resasco, J. Catal. 268 (2009) 68.
[16] M. Bejblova, P. Zamostny, L. Cerveny, J. Cejka, Collect. Czech. Chem. Commun. 68 (2003) 1969.
[17] R. Abu-Reziq, D. Avnir, J. Blum, J. Mol. Catal. A: Chem. 187 (2002) 277.
[18] M. Bejblova, P. Zamostny, L. Cerveny, J. Cejka, Appl. Catal. A: Gen. 296 (2005) 169.
[19] M.A. Vannice, D. Poondi, J. Catal. 169 (1997) 166.
[20] Z. Ji-lu, J. Anal. Appl. Pyrol. 80 (2007) 30.
[21] P. Kluson, L. Cerveny, J. Mol. Catal. A: Chem. 108 (1996) 107.
[22] F.H. Mahfud, F. Ghijsen, H.J. Heeres, J. Mol. Catal. A: Chem. 264 (2007) 227.
[23] A. Saadi, Z. Rassoul, M.M. Bettahar, J. Mol. Catal. A: Chem. 164 (2000) 205.
[24] Y. Roman-Leshkov, C.J. Barrett, Z.Y. Liu, J.A. Dumesic, Nat. Lett. 447 (2007) 982.
[25] H.Y. Zheng, Y.L. Zhu, B.T. Teng, Z.Q. Bai, C.H. Zhang, H.W. Xiang, Y.W. Li, J. Mol. Catal. A: Chem. 246 (2006) 18.
[26] R.D. Srivastava, A.K. Guha, J. Catal. 91 (1985) 254.
[27] T. Pham, S.P. Crossley, T. Sooknoi, L.L. Lobban, D.E. Resasco, R.G. Mallinson, Appl. Catal. A: Gen. 379 (2010) 135.
[28] J. Piskorza, D. Radlein, D.S. Scott, J. Anal. Appl. Pyrol. 9 (1986) 121.
[29] J.N. Chheda, Y. Román-Leshkov, J.A. Dumesic, Green Chem. 9 (2007) 342.
[30] T.Q. Hoang, X. Zhu, T. Danuthai, L.L. Lobban, D.E. Resasco, R.G. Mallinson, Energy Fuels 24 (2010) 3804.
[31] G. Kresse, J. Furthmueller, J. Phys. Rev. B 54 (1996) 11169.
[32] G. Kresse, J. Hafner, J. Phys. Rev. B 49 (1994) 14251.
[33] G. Kresse, J. Hafner, J. Phys. Rev. B 48 (1993) 13115.
[34] G. Kresse, J. Hafner, J. Phys. Rev. B 47 (1993) 558.
[35] G. Kresse, J. Furthmuller, Comput. Mater. Sci. 6 (1996) 5.
[36] G. Kresse, D. Joubert, J. Phys. Rev. B 59 (1999) 1758.
[37] P.E. Bloechl, J. Phys. Rev. B 50 (1994) 17953.
[38] J.P. Perdew, K. Burke, M. Ernzerhof, Phys. Rev. Lett. 77 (1996) 3865.
[39] F. Fouda-Onana, O. Savadogo, Electrochim. Acta 54 (2009) 1769.
[40] S. Barama, C.D. Batiot, M. Capron, E.B. Richard, O.B. Mohammedi, Catal. Today 141 (2009) 385.
[41] A.F. Gusovius, T.C. Watling, R. Prins, Appl. Catal. A: Gen. 188 (1999) 187.
[42] G. Aguila, F. Gracia, P. Araya, Appl. Catal. A: Gen. 343 (2008) 16.
[43] J. Batista, A. Pintar, D. Mandrino, M. Jenko, V. Martin, Appl. Catal. A: Gen. 206 (2001) 113.
[44] M. Fernandez-Garcia, G.L. Haller, J. de Phys. IV 7 (1997) 895.
[45] D. Gasparovicova, M. Kralik, M. Hronec, Z. Vallusova, H. Vinek, B. Corain, J. Mol. Catal. A: Chem. 264 (2007) 93.
[46] J. Kugai, J.T. Miller, N. Guo, C. Song, J. Catal. 277 (2011) 46.
[47] M. Primet, V. Mathieu, W.M.H. Sachtler, J. Catal. 44 (1976) 324.
[48] F. Skoda, M.P. Astier, G.M. Pajonk, M. Primet, Catal. Lett. 29 (1994) 159.
[49] S.S. Ashour, J.E. Bailie, C.H. Rochester, J. Thomson, G.J. Hutchings, J. Mol. Catal. A: Chem. 123 (1997) 65.
[50] F.B. Noronha, M. Schmal, M. Primet, R. Frety, Appl. Catal. 78 (1991) 125.
[51] M. Fernandez-Garcia, J.A. Anderson, G.L. Haller, J. Phys. Chem. 100 (1996) 16247.
[52] V. Ponec, Appl. Catal. A: Gen. 222 (2001) 31.
[53] A.B. Hungria, A. Iglesias-Juez, A. Martinez-Arias, M. Fernandez-Garcia, J.A. Anderson, J.C. Conesa, J. Soria, J. Catal. 206 (2002) 281.
[54] E. Jeroro, M.P. Hyman, J.M. Vohs, Phys. Chem. Chem. Phys. 11 (2009) 10457.
[55] B.L. Gustafson, P.S. Wehner, Appl. Surf. Sci. 52 (1991) 261.
[56] N. Martensson, R. Nyholm, H. Calen, J. Hedman, Phys. Rev. B 24 (1981) 1725.
[57] S. Sitthisa, T. Sooknoi, Y. Ma, P.B. Balbuena, D.E. Resasco, J. Catal. 277 (2011) 1.
[58] R. Shekhar, R.V. Plank, J.M. Vohs, M.A. Barteau, J. Phys. Chem. B 101 (1997) 7939.
[59] M.K. Bradley, J. bin Roson, D.P. Woodruff, Surf. Sci. 604 (2010) 920.
[60] M. Mavrikakis, M.A. Barteau, J. Mol. Catal. A: Chem. 131 (1998) 135.
[61] J.L. Davis, M.A. Barteau, J. Am. Chem. Soc. 111 (1989) 1782.
[62] J.L. Davis, M.A. Barteau, Surf. Sci. 235 (1990) 235.
[63] M.A. Henderson, Y. Zhou, J.M. White, J. Am. Chem. Soc. 111 (1989) 1185.
[64] R.J. Madix, T. Yamada, S.W. Johnson, Appl. Surf. Sci. 19 (1984) 13.
[65] B.A. Sexton, A.E. Hughes, N.R. Avery, Surf. Sci. 155 (1985) 366.
[66] J.B. Benziger, R.J. Madix, J. Catal. 65 (1980) 49.
[67] P.H. McBreen, W. Erley, H. Ibach, Surf. Sci. 133 (1983) 469.
[68] J. Hrbek, R.A. Depaola, F.M. Hoffmann, J. Chem. Phys. 81 (1984) 2818.
[69] J.E. Demuth, H. Ibach, Chem. Phys. Lett. 60 (1976) 395.
[70] S.R. Bare, J.A. Stroscio, W. Ho, Surf. Sci. 150 (1985) 399.
[71] R. Alcala, J. Greeley, M. Mavrikakis, J.A. Dumesic, J. Chem. Phys. 116 (2002) 8973.
[72] G.M.R. van Druten, V. Ponec, Appl. Catal. A: Gen. 191 (2000) 163.
[73] E. Jeroro, M.P. Hyman, J.M. Vohs, Phys. Chem. Chem. Phys. 11 (2009) 10457.
[74] H.L. Tierney, A.E. Baber, E.C.H. Sykes, J. Phys. Chem. C 113 (2009) 7246.
[75] J.C. Fernandez-Garcia, A. Conesa, J. Clotet, M. Ricart, N. Lopez, F. Illas, J. Phys. Chem. B 102 (1998) 141.
[76] N. Lopez, J.K. Norskov, Surf. Sci. 477 (2001) 59.
[77] G. Blyholder, J. Phys. Chem. 68 (1964) 2772.
[78] N.R. Avery, W.H. Weinberg, A.B. Anton, B.H. Toby, Phys. Rev. Lett. 51 (1983) 682.
[79] A.B. Anton, N.R. Avery, B.H. Toby, W.H. Weinberg, J. Am. Chem. Soc. 108 (1986) 684.
[80] H. Steininger, H. Ibach, S. Lehwald, Surf. Sci. 117 (1982) 685.
[81] J.F. Paul, P. Sautet, J. Phys. Chem. 98 (1994) 10906.